

Quantum particle on the surface of a cube

Darek Cidlinský^{1,*} and Tomáš Tyc¹

¹*Department of Theoretical Physics and Astrophysics, Faculty of Science,
Masaryk University, Kotlářská 2, 61137 Brno, Czechia*

We analyze dynamics of a quantum particle on a force-free surface of a cube. Employing methods of the group theory, we divide the solutions of the stationary Schrödinger equation (the modes) into classes based on irreducible representations of the symmetry group of the cube, and for each class we reduce the problem to finding the modes on a square with special boundary conditions. We analyze the properties of the resulting modes, present them visually, and discuss the possibility of quantum state revivals on the cube.

I. INTRODUCTION

Investigating solutions of the Schrödinger and Helmholtz equations on various spatial domains has attracted attention of the scientific community for a long time. It can directly be applied to solving quantum particle dynamics on such domains, or exploring vibrational modes of a membrane with a given shape. Usually, simply connected parts of a plane are analyzed, such as in the celebrated paper “Can one hear the shape of a drum?” [1]. The solutions of the stationary Schrödinger equation (the stationary states, or simply *modes*) can be employed for describing the full dynamics of the quantum particle on such a domain, or, in the related optical or mechanical case, of the electromagnetic or acoustic wave. The quantum spectrum has different properties for non-ergodic and ergodic systems; for the latter ones, such as, e.g., the stadium or Sinai dynamical billiard [2], the energy levels exhibit the typical level repulsion [3].

Quantum mechanics on curved surfaces such as the sphere has also attracted much attention in the previous decades. One possible approach to this problem is to consider quantum mechanics of a particle in \mathbb{R}^3 with an infinitely strong potential that forces it to move on the 2D surface [4]. The Hamiltonian in this case is proportional to the two-dimensional Laplacian corresponding to the kinetic energy on the surface, plus an additional term emerging from the constraint that the particle has to stay on the surface [4]. A different approach [5, 6] treats the surface as a 2D manifold from the beginning, without considering any particular embedding into the 3D Euclidean space. For the case of a polyhedron, this is equivalent to dealing with the individual flat polyhedron faces with appropriately identifying the corresponding edges. The Hamiltonian in this case is given purely by the kinetic energy on the surface that is proportional to the 2D Laplacian. Recently the surface of a regular tetrahedron [5] was analyzed in this way; it turned out that the modes can be found analytically and that the quantum state exhibits perfect revivals due to the fact that all energy levels are integer multiples of a common constant. Later, more exotic domains such the Möbius

strip, Klein’s bottle or the real projective plane were analyzed by the same method and it has been shown that the quantum wavefunction exhibits perfect revivals on these manifolds as well [6].

In this paper we employ the latter approach analyze quantum mechanics of a particle on another compact manifold, the surface of the cube. This manifold has already been analyzed in the setting of geometrical optics (and equivalently, classical mechanics), including photo-realistic simulations [7], but the case of a quantum particle on this surface has not been considered. Here we provide a complete solution of the stationary Schrödinger equation on this manifold, consisting of six unit squares whose edges and vertices are indentified in the appropriate way. Employing the group theory, we sort the modes into different classes according to their levels of degeneracy. Subsequently, we find the modes and energies for each class, analytically for some classes and semi-analytically for others. We also analyze the spectra of the modes and show that unlike the above mentioned manifolds, a general quantum wavepacket on the cube does not exhibit perfect quantum revivals.

The paper is organized as follows: In Sec. II we discuss the equations governing the quantum particle on the surface of the cube, in Sec. III we discuss the symmetry group of the cube and the resulting conditions for the modes corresponding to different irreducible representations, then in Secs. IV, V and VI we find the non-degenerate, double-degenerate and triple-degenerate modes, respectively. In Sec. VII we summarize the modes found, we discuss their properties in Sec. VIII, and we conclude in Sec. IX.

II. SCHRÖDINGER EQUATION ON THE SURFACE OF THE CUBE

We start with the Schrödinger equation for a particle moving on a potential-free surface of the unit cube,

$$i\hbar \frac{\partial \Psi}{\partial t} = \hat{H} \Psi = -\frac{1}{2m} \Delta \Psi. \quad (1)$$

Here the Hamiltonian consists purely of the kinetic energy term, $-\Delta/(2m)$, where Δ is the two-dimensional Laplace operator. Separating the time variable as

* darek@mail.muni.cz

$\Psi(\vec{r}, t) = \psi(\vec{r}) \exp(-iEt/\hbar)$, where E is the particle energy, and working in the units where the Planck's constant \hbar and the particle's mass m are equal to unity, we get the stationary Schrödinger equation for ψ in the form

$$\Delta\psi + 2E\psi = 0. \quad (2)$$

Here, the wavefunctions ψ belong to the Hilbert space of functions that are square-integrable over the six faces of the cube and satisfy the appropriate boundary conditions corresponding to the edge identification. The scalar product is defined in the usual way, $\langle f|g \rangle = \sum_{n=1}^6 \iint_{n\text{-th face}} f^* g dx dy$, and the Hamiltonian is Hermitian with respect to this product.

Finding the eigenstates (modes) ψ_i and the corresponding eigenvalues E_i of Eq. (2) completely determines the quantum dynamics of the particle. Moreover, since Eq. (2) represents at the same time the Helmholtz equation that governs scalar waves in a medium with a constant refractive index, finding the modes of Eq. (2) also solves the dynamics of light confined to a geodesic lens [8, 9], in this case in the form of a cube.

Due to the compactness of the manifold, the spectrum $\{E_i\}$ is discrete and the eigenmodes are countable. One option for finding the modes would be to unwrap the surface of the cube into its unfolded net, and look for the solutions of Eq. (2) on this planar domain with the appropriate boundary conditions that involve the continuity and smoothness of the solution when going from one face to another via their common edge. However, here we pursue a different strategy. We divide each face of the cube into eight triangles using the axes of the face edges and its diagonals as shown in Fig. 1(a). This yields the total of 48 triangles for the whole cube, each of which is joined to other three via its sides. Solving the Helmholtz equation on the surface of the cube then reduces to solving it on each triangle and matching these solutions together so that both the combined solution and its normal derivative is continuous on the sides connecting any two triangles. In the next section, we establish a set of rules for matching the solutions on the triangles together using the group theory.

III. SYMMETRY GROUP OF THE CUBE

As it is well known, the cube has a symmetry group of $\mathbb{S}_4 \times \mathbb{Z}_2$, called also the *octahedral group*. It has 48 elements (24 rotations and 24 roto-reflections). By applying a suitable element of the group, any of the 48 triangles defined in the previous section can be transformed to any other triangle. Moreover, a particular representation of the group reveals how the modes belonging to this representation are transformed among themselves when the symmetry operations are applied to them. This way, if we obtain a solution on one of those little triangles with suitable properties, we can use this information to extend it to the whole cube. Hence, one such little triangle will be called the *fundamental domain*, see Fig. 1.

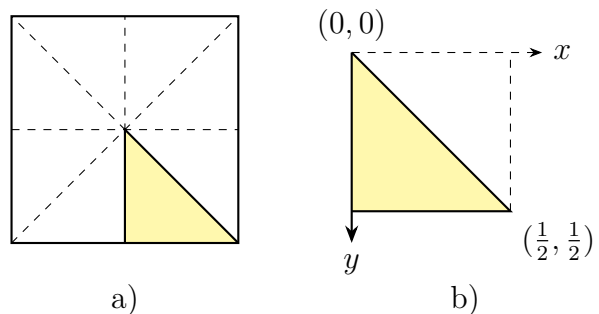


FIG. 1. **a)** One face of the unit cube divided into 8 isosceles triangles. One of them, picked to be the fundamental domain, is highlighted. **b)** To facilitate solution, we solve the equation on two adjacent triangles. We use coordinates x, y as shown in the picture.

It is also well known that the octahedral group has 10 irreducible representations in total. These can, for instance, explicitly be found using the GAP software. The character table of the octahedral group is shown in Tab. I.

	1	8	C_3	6	C_2	6	C_4	3	C_4^2	R	6	S_4	8	S_6	3	σ_h	6	σ_d
A_{1g}	1	1	1	1	1	1	1	1	1	1	1	1	1	1	1	1	1	1
A_{2g}	1	1	-1	-1	1	1	-1	-1	1	1	-1	1	1	1	-1	-1	1	-1
A_{1u}	1	1	1	1	1	1	-1	-1	-1	-1	-1	-1	-1	-1	-1	-1	-1	-1
A_{2u}	1	1	-1	-1	1	1	-1	-1	1	-1	1	-1	-1	-1	1	1	1	1
E_g	2	-1	0	0	2	2	0	0	-1	2	0	-1	2	0	0	0	0	0
E_u	2	-1	0	0	2	-2	0	0	1	-2	0	1	-2	0	0	0	0	0
T_{1g}	3	0	-1	1	-1	3	1	0	-1	-1	0	-1	-1	-1	1	1	1	1
T_{2g}	3	0	1	-1	-1	3	-1	0	-1	1	0	-1	1	0	-1	1	1	1
T_{1u}	3	0	-1	1	-1	-3	-1	0	1	1	0	1	1	0	1	1	1	1
T_{2u}	3	0	1	-1	-1	-3	1	0	1	1	0	1	1	0	1	1	1	1

TABLE I. The character table for the octahedral group.

The table reveals that there are four one-dimensional, two two-dimensional and four three-dimensional irreducible representations of the group. Since the dimensionality of the representation is equal to the degree of degeneracy of the modes, we see that there will be four different types of non-degenerate modes, two types of double-degenerate modes, and four types of triple-degenerate modes.

Before we can reduce the problem to solving the Helmholtz equation on the fundamental domain, we must obtain the appropriate boundary conditions — for each irreducible representation, a certain set of boundary conditions must be used, and it is not *a priori* obvious what they are. Fortunately, we can obtain the conditions with the help of a simple proposition that holds generally, without any special reference to the cube.

Proposition. *Let f_1, f_2, \dots, f_n be a set of basis functions defined in a region of a plane, and let \mathcal{R} be an operation of a reflection through a straight line l in that region. If $\mathcal{R}f_k = \mathcal{M}_{kl}f_\ell$ (we are using Einstein's*

convention, summing over repeated indices), then:

1. If c_k is an eigenvector of the matrix \mathcal{M}^T with the eigenvalue -1 (i.e., $M_{k\ell}c_k = -c_\ell$), then $c_k f_k = 0$ on the line l .
2. If c_k is an eigenvector of \mathcal{M}^T with the eigenvalue $+1$, then the normal (with respect to l) derivative of the function $c_k f_k$ is zero on the line l .

Proof: First consider the function $f = c_k f_k$ corresponding to an eigenvector of \mathcal{M}^T with the eigenvalue -1 . Upon reflection in the line l , this function changes to $\tilde{f} = \mathcal{R}f = c_k \mathcal{R}f_k = c_k M_{k\ell} f_\ell = -c_\ell f_\ell = -f$. At the same time, on the line l itself we must have $\tilde{f} = f$ because l changes into itself upon reflection in l . Combining these two properties of the functions f and \tilde{f} , we see that $f = 0$ on the line l .

Similarly, consider the function $f = c_k f_k$ corresponding to an eigenvector of \mathcal{M}^T with the eigenvalue $+1$. Upon reflection in the line l , this function changes to $\tilde{f} = \mathcal{R}f = c_k \mathcal{R}f_k = c_k M_{k\ell} f_\ell = c_\ell f_\ell = f$, i.e., to itself, and consequently its normal derivative, $\partial f / \partial \vec{n}$, flips sign. By a similar argument as before we then see that $\partial f / \partial \vec{n} = 0$ on the line l . ■

IV. NON-DEGENERATE MODES

First we analyze the non-degenerate modes, corresponding to the first four lines in character table, Tab. I. From the table we can find how the modes behave if we reflect the fundamental domain through one of its sides. We can summarize this graphically as in Fig. 2. The numbers shown are the “representation matrices” for the reflections, in this case 1×1 : if we perform a reflection through a given side, the mode will be multiplied by the corresponding number. From the Proposition it then follows that all the “ -1 ”s imply a boundary condition of $f = 0$ for the modal function while all “ $+1$ ”s imply $\partial f / \partial \vec{n} = 0$.

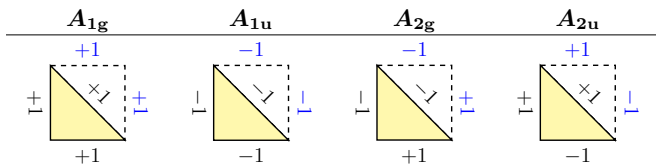


FIG. 2. Transformations of the modal functions upon reflections in the sides of the fundamental domain, according to the representation the function belongs to. The black numbers indicate whether the modal function remains unchanged ($+1$) or flips the sign (-1) upon the reflection. A second little triangle, marked by a dashed line, is added as in Fig. 1. The blue numbers have the same meaning for these added triangles as the black numbers have for the fundamental domain.

We add a second little triangle to make a square (as indicated in Fig. 1(b)) and start solving the equations.

For the representation A_{1g} , we must solve the Helmholtz equation on the square with normal derivatives vanishing at the edges. The solution is easily shown to be $\cos(2\pi kx) \cos(2\pi \ell y)$ with $k, \ell \in \mathbb{N}_0$, where the Cartesian coordinate system xy for the fundamental domain is depicted in Fig. 1(b). However, the reflection through the diagonal (effected by interchanging x and y) must leave the mode invariant since there is “ $+1$ ” on the diagonal, so the only solution that we can accept as a mode is a sum of the above solution with its reflected version. This gives the mode in the form

$$\psi^{(A_{1g})} = \cos(2\pi kx) \cos(2\pi \ell y) + \cos(2\pi \ell x) \cos(2\pi ky), \quad (3)$$

with the energy eigenvalue $E = \frac{\pi^2}{2} [(2k)^2 + (2\ell)^2]$.

The other three cases can be analyzed in the same fashion. For the representation A_{1u} , we obtain

$$\psi^{(A_{1u})} = \sin(2\pi kx) \sin(2\pi \ell y) - \sin(2\pi ky) \sin(2\pi \ell x), \quad (4)$$

again with $E = \frac{\pi^2}{2} [(2k)^2 + (2\ell)^2]$. However, we can easily see that if $k = 0, \ell = 0$ or $k = \ell$, the formula will yield an identical zero. Therefore, in the representation A_{1u} , we only have modes when $k \neq 0, \ell \neq 0, k \neq \ell$.

Next, for A_{2g} we have

$$\psi^{(A_{2g})} = \cos[(2k+1)\pi x] \cos[(2\ell+1)\pi y] - \cos[(2\ell+1)\pi x] \cos[(2k+1)\pi y] \quad (5)$$

with $E = \frac{\pi^2}{2} [(2k+1)^2 + (2\ell+1)^2]$. Once again, there is no mode for $k = \ell$. Finally for A_{2u} we find

$$\psi^{(A_{2u})} = \sin[(2k+1)\pi x] \sin[(2\ell+1)\pi y] + \sin[(2\ell+1)\pi x] \sin[(2k+1)\pi y] \quad (6)$$

with $E = \frac{\pi^2}{2} [(2k+1)^2 + (2\ell+1)^2]$.

These results, along with other modes, are summarized in Table II. in section VII.

V. DOUBLE-DEGENERATE MODES

To analyze the case of double-degenerate modes, we proceed in a similar fashion as for the non-degenerate modes. However, now there are two independent modes f and g for each energy, so the sides of the fundamental domain will be labelled by 2×2 matrices as in Fig. 3. They show how the modes change due to the reflection \mathcal{R} through the given side in the manner used in the Proposition, i.e., $\begin{pmatrix} \mathcal{R}f \\ \mathcal{R}g \end{pmatrix} = \mathcal{M} \begin{pmatrix} f \\ g \end{pmatrix}$.

We start with the modes E_g . We will find the eigenvectors and eigenvalues of the matrices the sides are labeled with, and translate them into boundary conditions using the Proposition; then we add a second triangle to the fundamental domain to make a square, and proceed with the solution on the square. All in all, we obtain a boundary problem characterized by Fig. 4. In order to solve

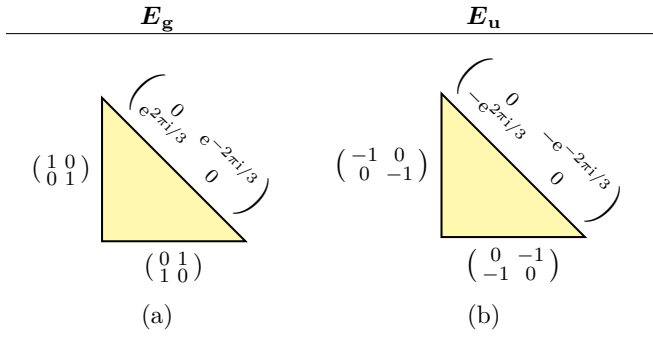


FIG. 3. The relevant representation matrices for the two-dimensional irreducible representations, (a) E_g and (b) E_u . There is a basis of the 2D eigenspace of the Laplacian that transforms with these matrices when the functions are reflected through the given side of the triangle.

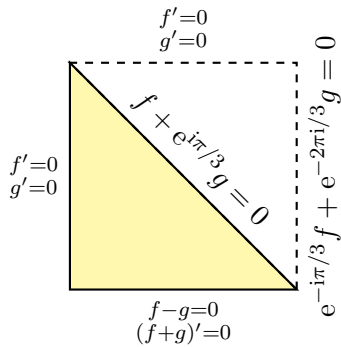


FIG. 4. Boundary conditions obtained for the basis functions of the E_g representation. The prime is used as an abbreviation for the the normal derivative.

the problem, we would like to construct functions that have simple boundary conditions on at least three sides of the square. For this purpose, it is useful to introduce an alternative basis

$$\psi = f - g, \quad \varphi = e^{-i\pi/3}f + e^{-2\pi i/3}g.$$

According to the representation matrix in Fig. 3(a), the reflection \mathcal{R} in the diagonal acts as $\mathcal{R}f = e^{-2\pi i/3}g$ and $\mathcal{R}g = e^{2\pi i/3}f$, which implies $\mathcal{R}\psi = e^{-2\pi i/3}g - e^{2\pi i/3}f = \varphi$. This way, the function φ can be obtained simply by reflecting the function ψ through the diagonal, which can also be expressed as $\psi(y, x) = \varphi(x, y)$. This results in significantly simpler conditions for the functions ψ and φ on three sides of the square than there would be for f and g ; these conditions are summarized in Fig. 5(a).

In particular, we know that $\partial\varphi/\partial x = 0$ on the line $x = 0$, and $\varphi = 0$ on the line $x = 1/2$. A function of x that satisfies these conditions has the form $\cos[(2k + 1)\pi x]$, $k \in \mathbb{N}$, and this function has to be multiplied by a suitable function of y so that the total energy amounts to given, but yet unknown constant E . Since φ must have zero normal derivative at $y = 0$, this function must be of the form $\cos(Cy)$. Hence, we may write the solution as a

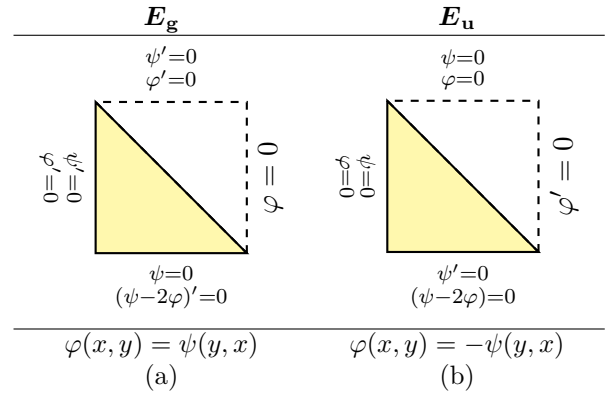


FIG. 5. Boundary conditions for the new basis φ, ψ for both two-dimensional representations.

series

$$\varphi^{(E_g)} = \sum_{k=0}^{\infty} c_k \cos[(2k+1)\pi x] \cos\left[\sqrt{2E - (2k+1)^2\pi^2}y\right]. \quad (7)$$

In the sum, for k sufficiently large the number under the square root goes negative; then the root itself becomes purely imaginary, which turns the trigonometric functions \cos into the hyperbolic function \cosh . Such terms (we will call them *evanescent terms*) have to be included in the sum as well; however, it turns out that only the first few such terms are non-negligible.

The possible values of E will be found from the extra boundary condition. As seen from Fig. 5(a), the condition is $\frac{\partial}{\partial y}(\psi - 2\varphi)\Big|_{y=1/2} = 0$, where $\psi(x, y) = \varphi(y, x)$. This can be expressed as an equation of the form $\sum_{k=0}^{\infty} c_k g_k(x; E) = 0$ for some functions g_k . This means that the energies will be precisely the values E for which the set of functions $g_k(x; E)$ is linearly dependent (as functions of x). We do not attempt to find them exactly; instead, we truncate the sum after a suitable number of terms (usually terminating the series after three evanescent terms gives highly satisfactory results, see also Appendix A), expand each of the g_k into a suitable Fourier basis, and, using the singular value decomposition, we numerically find the energies for which the g_k 's are “closest to being linearly dependent”. The details can be found in Appendix A. The result of our procedure are the energies and the corresponding expansion coefficients c_k that determine the wavefunctions in terms of Eq. (7).

The case of the representation E_u is solved in a similar fashion: we define functions ψ and φ in the same way as before and find for them the boundary conditions shown in Fig. 5(b). Subsequently, we express the wavefunction as

$$\varphi^{(E_u)} = \sum_{k=0}^{\infty} c_k \sin[(2k+1)\pi x] \sin\left[\sqrt{2E - (2k+1)^2\pi^2}y\right] \quad (8)$$

with an additional condition that $[\varphi - 2\psi]_{y=1/2} = 0$,

where $\psi(x, y) = -\varphi(y, x)$. By the procedure described above we again find the energies and the corresponding expansion coefficients c_k . The resulting modes are presented in Sec. VII.

VI. TRIPLE-DEGENERATE MODES

To analyze the triply degenerate modes corresponding to the representations T_{1g}, T_{1u}, T_{2g} and T_{2u} , we repeat the same process once again. Fig. 6 shows the relevant representation matrices, where “ \pm ” means “ $+$ ” for the “g” representations, and “ $-$ ” for the “u” representations.

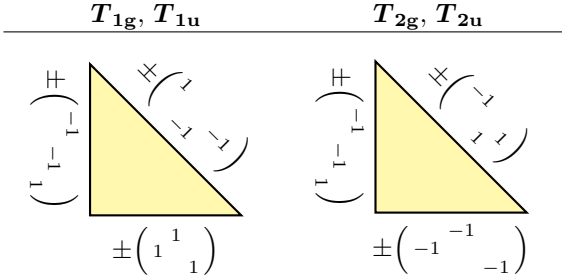


FIG. 6. The relevant representation matrices for all four three-dimensional irreducible representations. In “ \pm ”, the plus and minus signs apply to the “g” and “u” representations, respectively.

Denote the three basis functions by f, g, h . Using the Proposition, we arrive at boundary conditions for them that are summarized in Fig. 7.

Let us start with T_{1g} . We see that for g , we already have simple boundary conditions on three sides of the square. Hence, we may write down the solution as a series

$$g^{(T_{1g})} = \sum_{k=0}^{\infty} d_k \sin[(2k+1)\pi x] \times \cos \left[\sqrt{2E - (2k+1)^2\pi^2} y \right]. \quad (9)$$

Obtaining a solution for the function f is more complicated. We only have two simple boundary conditions: f must be zero on $x = 0$ and $y = 0$, so it is a linear combination of products of two sines in the form $\sin K_1 x \sin K_2 y$ with arbitrary $K_{1,2}$ (even imaginary) satisfying $K_1^2 + K_2^2 = 2E$. Hence, f can be any function of the following form:

$$f^{(T_{1g})} = \int_{-\infty}^{\infty} d\lambda c(\lambda) \sin(\sqrt{\lambda} x) \sin(\sqrt{2E - \lambda} y). \quad (10)$$

Additionally, f and g must be equal on the bottom side where $y = 1/2$. Since g is a series in $\sin[(2k+1)\pi x]$, we demand f to be the same kind of series, too, i.e., $\sum c_n \sin[(2n+1)\pi x]$, on that side. However, there is also

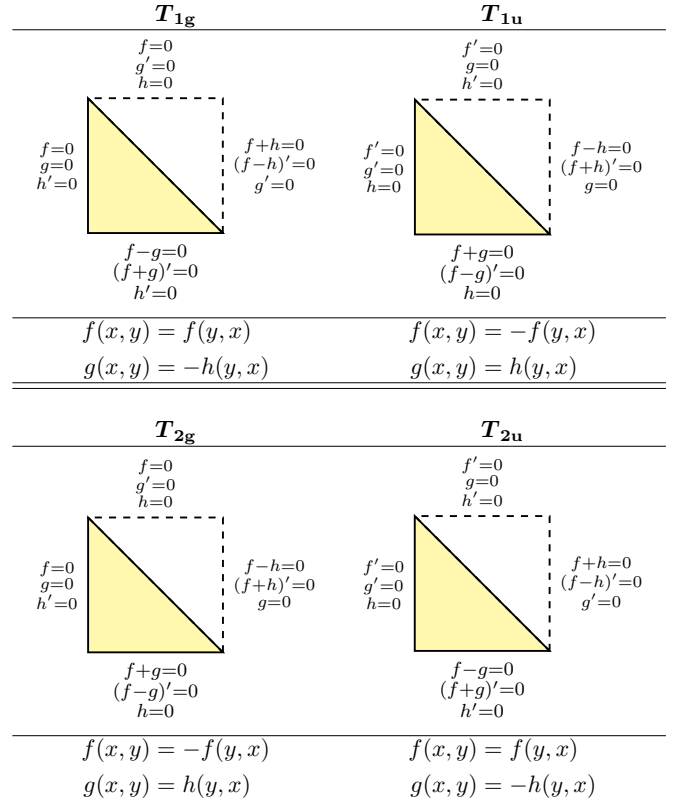


FIG. 7. Boundary conditions for the three basis functions f, g, h of all four three-dimensional irreducible representations and additional relations between the functions.

a requirement that f must not change when we reflect through the diagonal. Therefore we use the following ansatz for f :

$$f^{(T_{1g})} = \sum_{k=0}^{\infty} c_k \left\{ \sin[(2k+1)\pi x] \sin[\sqrt{2E - (2k+1)^2\pi^2} y] + \sin[(2k+1)\pi y] \sin[\sqrt{2E - (2k+1)^2\pi^2} x] \right\}. \quad (11)$$

It may look like this solution will not match g on the account of the factors $\sin \sqrt{(\dots)} x$. However, we use the fact that the functions $2 \sin[(2k+1)\pi x]$ are orthonormal on the interval $[0, 1/2]$ with respect to the inner product $\langle f|g \rangle = \int_0^{1/2} f^* g dx$. That makes it possible to expand the offending sine into a series in $\sin[(2k+1)\pi x]$ as well:

$$\sin \left[\sqrt{2E - (2n+1)^2\pi^2} x \right] = 4\sqrt{2E - (2n+1)^2\pi^2} \cos \left(\frac{1}{2} \sqrt{2E - (2n+1)^2\pi^2} \right) \times \sum_{k=0}^{\infty} \frac{(-1)^k \sin[(2k+1)\pi x]}{\pi^2 [(2k+1)^2 + (2n+1)^2] - 2E}. \quad (12)$$

Hence our ansatz can be still rewritten as a series in $\sin[(2k+1)\pi x]$, so it can be accepted as the most general form of f .

Now we have two sets of coefficients, c_k and d_k , and two conditions: on the bottom side, we must have both $f = g$ and $f' = -g'$. This way, we must find twice as many coefficients as in the case of double-degenerate modes, but we also have twice as many equations available. The procedure is the same as before — the energies are precisely the values of E for which we can find nonzero c_k and d_k such that the two conditions are fulfilled, and c_k, d_k themselves determine the modes.

Similar solutions can be obtained for the remaining representations as well. All are summarized in Table II in section VII, along with formulae that we derived for all other representations.

VII. DISCUSSION OF THE MODE PROPERTIES

The modes derived above in Sections IV—VI are summarized in Table II. In the following, we describe some general properties of the modes belonging to different representations. These properties can be derived from the symmetry analysis of the modes, and they are also clearly visible on the examples of modal functions plotted on the net of the cube in Figs. 8—11 as well as in the mode gallery in Sec. VIII.

The first observation is that the non-degenerate modes A_{1g}, A_{1u}, A_{2g} and A_{2u} look the same on all the cube faces, see Fig. 8. The modes A_{1u} and A_{2g} vanish on the cube edges while the modes A_{1g} and A_{2u} have zero normal derivative on the edges. The modes A_{1u}, A_{2g} and A_{2u} vanish at the cube face centers while the modes A_{1g} have there local extrema.

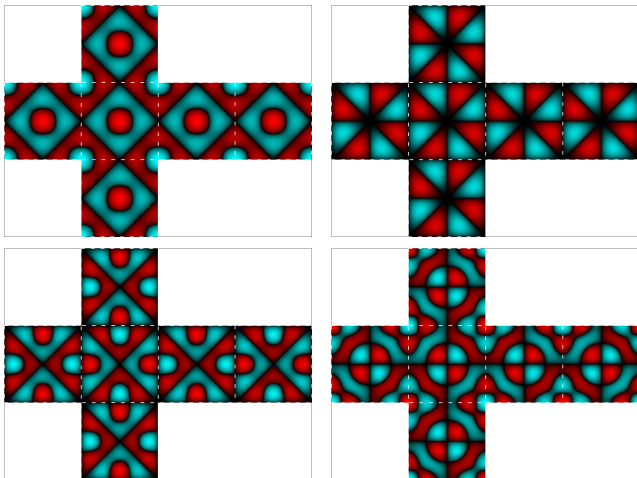


FIG. 8. Examples of non-degenerate modes. First row: A_{1g}, A_{1u} . Second row: A_{2g}, A_{2u} . All four cases correspond to $k = 2, \ell = 1$. The modal functions on different faces are always the same (in some cases, apart from a rotation by $\pi/2$). In this and all subsequent pictures, brightness corresponds to the amplitude, and hue to the phase. Since the non-degenerate modes are real, we only have red hue for positive and cyan for negative values.

The double-degenerate modes can be represented either using the functions ψ, φ that are real, or these two can be combined back to make the original basis f, g . The latter functions are complex, and in fact they satisfy $g = -f^*$. Let us discuss them further.

As follows from the analysis and can be seen in Fig. 9, the modes f (and equivalently g) are the same on the cube faces up to phase factors of $e^{\pm 2\pi i/3}$. This corresponds to the mode picking up these phases when rotated by $\pm 2\pi/3$ radians around the space diagonals of the cube. Expressed differently, there is a phase singularity (analogous to an optical vortex [10]) at each vertex of the cube. When switching from a given mode f to its partner g , the sign of this phase singularity (topological charge [10]) reverses because, as we have mentioned, the mode f is the complex conjugate of $-g$.

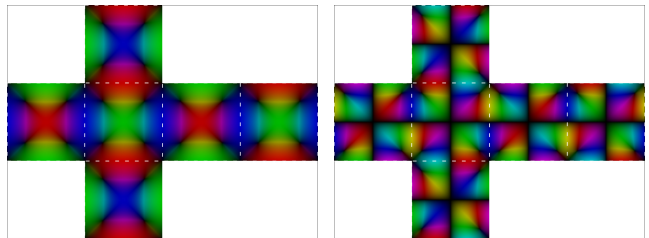


FIG. 9. Examples of double-degenerate modes for the representations E_g and E_u . The modal functions on different faces are the same up to phase factors of $e^{\pm 2\pi i/3}$. Both pictures show one of the basis function f, g . The other one can be found using the relation $g = -f^*$.

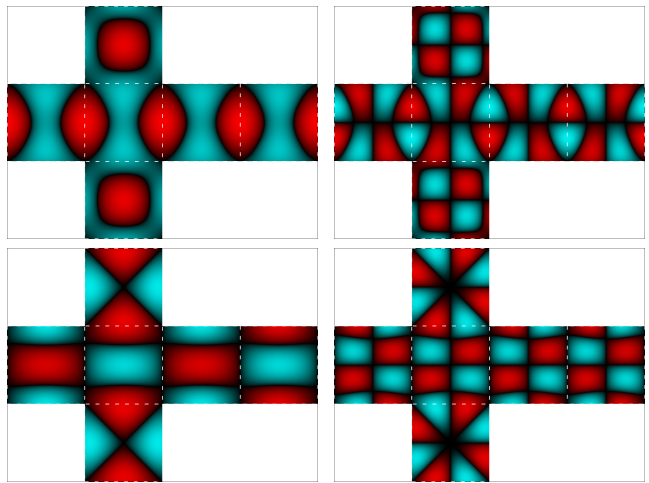


FIG. 10. An alternative representation of the double-degenerate modes shown in Fig. 9. Each row shows the real part u and the imaginary parts v , respectively, of f for the E_g mode (first row) and the E_u mode (second row). The modal functions look different on the polar faces (the squares at the top and bottom of the net) and on the equatorial faces (the squares in the middle row).

Alternatively, one could also present the double-degenerate modes using the original functions f, g . How-

\mathbf{A}_{1g}	$\cos[2k\pi x] \cos[2\ell\pi y] + \cos[2k\pi y] \cos[2\ell\pi x]$	$E = \frac{1}{2}\pi^2[(2k)^2 + (2\ell)^2]$
\mathbf{A}_{1u}	$\sin[2k\pi x] \sin[2\ell\pi y] - \sin[2k\pi y] \sin[2\ell\pi x]$	$E = \frac{1}{2}\pi^2[(2k)^2 + (2\ell)^2]$; k, ℓ nonzero and different
\mathbf{A}_{2g}	$\cos[(2k+1)\pi x] \cos[(2\ell+1)\pi y] - \cos[(2\ell+1)\pi x] \cos[(2k+1)\pi y]$	$E = \frac{1}{2}\pi^2[(2k+1)^2 + (2\ell+1)^2]$; k and ℓ different
\mathbf{A}_{2u}	$\sin[(2k+1)\pi x] \sin[(2\ell+1)\pi y] + \sin[(2\ell+1)\pi x] \sin[(2k+1)\pi y]$	$E = \frac{1}{2}\pi^2[(2k+1)^2 + (2\ell+1)^2]$
\mathbf{E}_g	$\varphi = \sum_{k=0}^{\infty} c_k \cos[(2k+1)\pi x] \cos\left[\sqrt{2E - (2k+1)^2\pi^2} y\right]$	with $\frac{\partial}{\partial y}(\psi - 2\varphi)\Big _{y=1/2} = 0$, where $\psi(x, y) = \varphi(y, x)$.
\mathbf{E}_u	$\varphi = \sum_{k=0}^{\infty} c_k \sin[(2k+1)\pi x] \sin\left[\sqrt{2E - (2k+1)^2\pi^2} y\right]$	with $\psi(x, \frac{1}{2}) - 2\varphi(x, \frac{1}{2}) = 0$, where $\psi(x, y) = -\varphi(y, x)$.
\mathbf{T}_{1g}	$f = \sum_{k=0}^{\infty} c_k \left\{ \sin[(2k+1)\pi x] \sin\left[\sqrt{2E - (2k+1)^2\pi^2} y\right] \right.$ $\left. + \sin[(2k+1)\pi y] \sin\left[\sqrt{2E - (2k+1)^2\pi^2} x\right] \right\}$ $g = \sum_{k=0}^{\infty} d_k \sin[(2k+1)\pi x] \cos\left[\sqrt{2E - (2k+1)^2\pi^2} y\right]$	with $f(x, \frac{1}{2}) - g(x, \frac{1}{2}) = 0$, $\frac{\partial}{\partial y}(f+g)\Big _{y=1/2} = 0$ $h(x, y) = -g(y, x)$
\mathbf{T}_{1u}	$f = \sum_{k=0}^{\infty} c_k \left\{ \cos[(2k+1)\pi x] \cos\left[\sqrt{2E - (2k+1)^2\pi^2} y\right] \right.$ $\left. - \cos[(2k+1)\pi y] \cos\left[\sqrt{2E - (2k+1)^2\pi^2} x\right] \right\}$ $g = \sum_{k=0}^{\infty} d_k \cos[(2k+1)\pi x] \sin\left[\sqrt{2E - (2k+1)^2\pi^2} y\right]$	with $f(x, \frac{1}{2}) + g(x, \frac{1}{2}) = 0$, $\frac{\partial}{\partial y}(f-g)\Big _{y=1/2} = 0$ $h(x, y) = g(y, x)$
\mathbf{T}_{2g}	$f = \sum_{k=0}^{\infty} c_k \left\{ \sin[2k\pi x] \sin\left[\sqrt{2E - \pi^2 k^2} y\right] \right.$ $\left. - \sin[2k\pi y] \sin\left[\sqrt{2E - (2k)^2\pi^2} x\right] \right\}$ $g = \sum_{k=0}^{\infty} d_k \sin[2k\pi x] \cos\left[\sqrt{2E - (2k)^2\pi^2} y\right]$	with $f(x, \frac{1}{2}) + g(x, \frac{1}{2}) = 0$, $\frac{\partial}{\partial y}(f-g)\Big _{y=1/2} = 0$ $h(x, y) = g(y, x)$
\mathbf{T}_{2u}	$f = \sum_{k=0}^{\infty} c_k \left\{ \cos[2k\pi x] \cos\left[\sqrt{2E - \pi^2 k^2} y\right] \right.$ $\left. + \cos[2k\pi y] \cos\left[\sqrt{2E - (2k)^2\pi^2} x\right] \right\}$ $g = \sum_{k=0}^{\infty} d_k \cos[2k\pi x] \sin\left[\sqrt{2E - (2k)^2\pi^2} y\right]$	with $f(x, \frac{1}{2}) - g(x, \frac{1}{2}) = 0$, $\frac{\partial}{\partial y}(f+g)\Big _{y=1/2} = 0$ $h(x, y) = -g(y, x)$

TABLE II. Table of the modes of the cube corresponding to all irreducible representations of the octahedral group.

ever, a still slightly different mode basis is more useful for their visual presentation, namely the real and imaginary parts of the function f that we can denote by u and v , respectively. The resulting modes have different properties than f and g themselves. In particular, for each of u and v there are two types of faces: two mutually opposite faces (we will call them “polar faces”) that look the same, and the remaining four faces (we will call them “equatorial faces”) that again look the same as one another (up to a possible sign flip) but different than the polar faces, see Fig. 10. Obviously, one could rotate these modes around the space diagonals to change the position of the polar faces without changing the energy of the state. This way, one can obtain six different states, three for u and three for v , differing by polar face positions; still only two of these six states are linearly independent.

Next we proceed to triple-degenerate modes. Their general character is the same as described above for the double-degenerate modes u and v , so for each mode f , g

or h there are two polar and four equatorial faces. Unlike the double-degenerate case, however, now the three possible choices of polar face positions correspond precisely to the three linearly independent modes f , g and h .

We will also discuss an interesting question whether the quantum particle on the surface of the cube exhibits quantum state revivals. Such revivals are present in a quantum system if all the energy levels are integer multiples of some common constant (with an optional global additive constant) because then after a certain time T (the revival time), all the modes acquire a phase that is an integer multiple of 2π , so the initial quantum state is perfectly recovered. Perfect quantum revivals are present for a particle in an infinite potential well in the shape of a square, on a flat torus, on a sphere [11], on the surface of a tetrahedron [5], on the Möbius strip, Klein’s bottle and the real projective plane [6], to name some examples. However, the surface of the cube does not have this property in general. The energy spectrum, apart from

the analytically derived non-degenerate levels, does not follow the above rule, so perfect quantum revivals cannot be expected. However, the nondegenerate levels alone do observe the above rule because their energies are integer multiples of π^2 (see Sec. IV or Table II), which gives the revival time $T = 2/\pi$. This way, special wavepackets on the cube containing only the non-degenerate modes would exhibit perfect quantum state revivals.

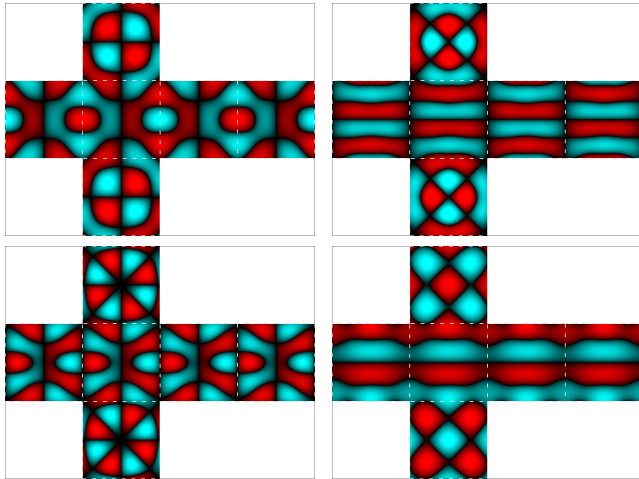


FIG. 11. Examples of triple-degenerate modes. First row: T_{1g} , T_{1u} . Second row: T_{2g} , T_{2u} . One of the three basis functions f , g , h is shown. The remaining modes g and h from the same level differ just by polar face positions.

VIII. GALLERY OF MODES

In Figs. 12—21 we present a gallery of modes, showing a perspective view of the cube. We show the eight lowest modes for each irreducible representation along with the energy values (exact for the non-degenerate modes and numerically calculated for the degenerate modes). For the triple-degenerate modes whose polar and equatorial faces differ, one of the polar faces is at the top. The general properties discussed in Sec. VII can clearly be seen.

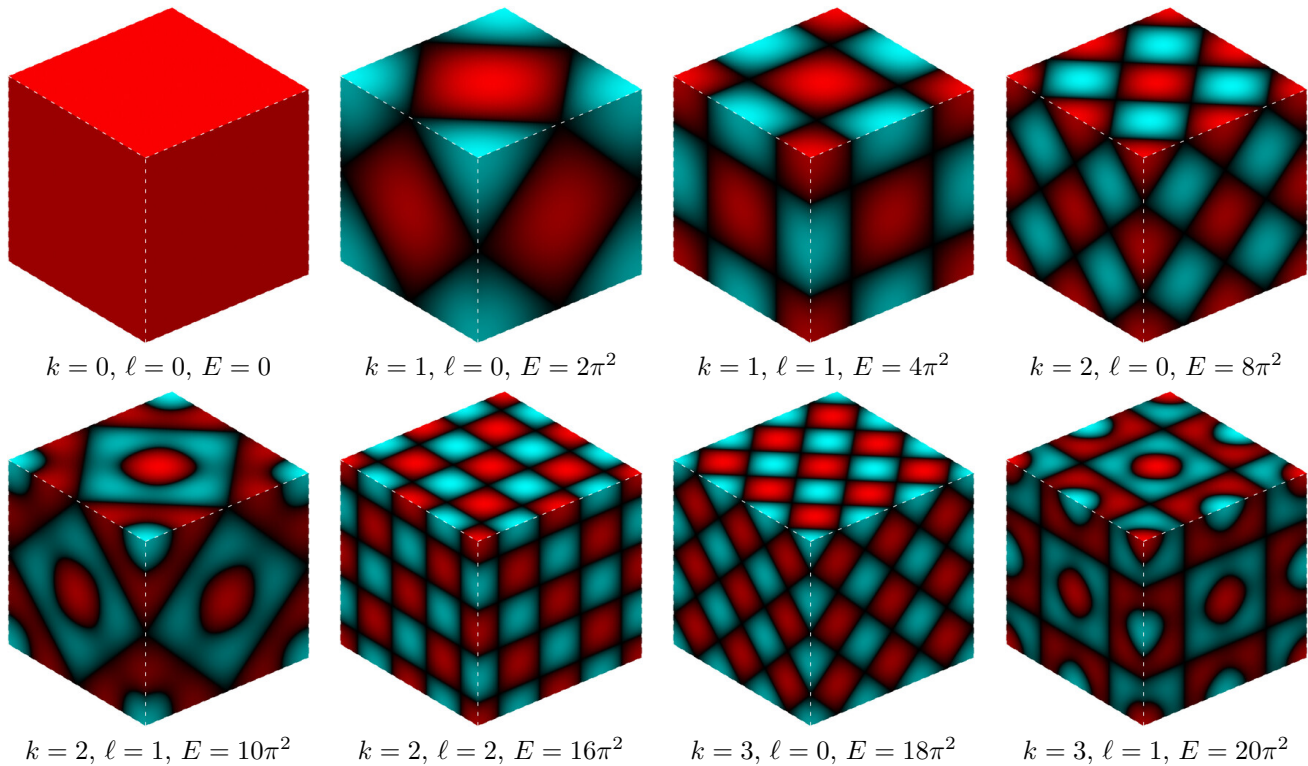


FIG. 12. The first eight modes for the irreducible representation A_{1g} .

IX. CONCLUSION

In conclusion, we have found a simple but powerful method for solving the Schrödinger (or equivalently, Helmholtz) equation on the surface of the cube. Using the representation matrices of the octahedral group, we were able to break down the problem into 10 different cases, corresponding to the 10 irreducible representations of the group, and we obtained appropriate boundary conditions that enable us to reduce the solution to just 1/8 of one face. Then, it was sufficient to solve a boundary problem on a planar region, namely a square, as opposed to a complicated manifold like the surface of the cube.

In the case of one-dimensional representations, we have obtained analytic expressions for the modes and their energies. In the other cases, we have been able to express the modes semi-analytically, in the form of a sum with unknown coefficients that need to be found numerically. We have developed a computer procedure for performing this task, allowing us to calculate as many modes and their energies as required, with a good degree of accu-

racy. The expressions for the modes belonging to all representations were summarized in Table II, and a gallery of modes was presented in Sec. VIII.

We have also shown that a general quantum wavepacket on the cube does not exhibit perfect quantum revivals; only specially prepared states do.

Finally, we note that the method developed here is very general and it may be used for studying the modes of different polyhedra as well. Its success depends only on one's ability to solve the Helmholtz equation on the corresponding planar fundamental domain. For instance, it could be used to find at least some modes of the octahedron and the icosahedron, since they consist of equilateral triangles, and solutions of Helmholtz equation on an equilateral triangle are known.

Our procedure may be adapted to the approach followed by da Costa [4] of restricting the 3D quantum mechanical problem to the 2D surface, as mentioned in the Introduction. There, an additional term would appear in the Schrödinger equation that contains the mean and Gauss curvatures. This would result in appearance

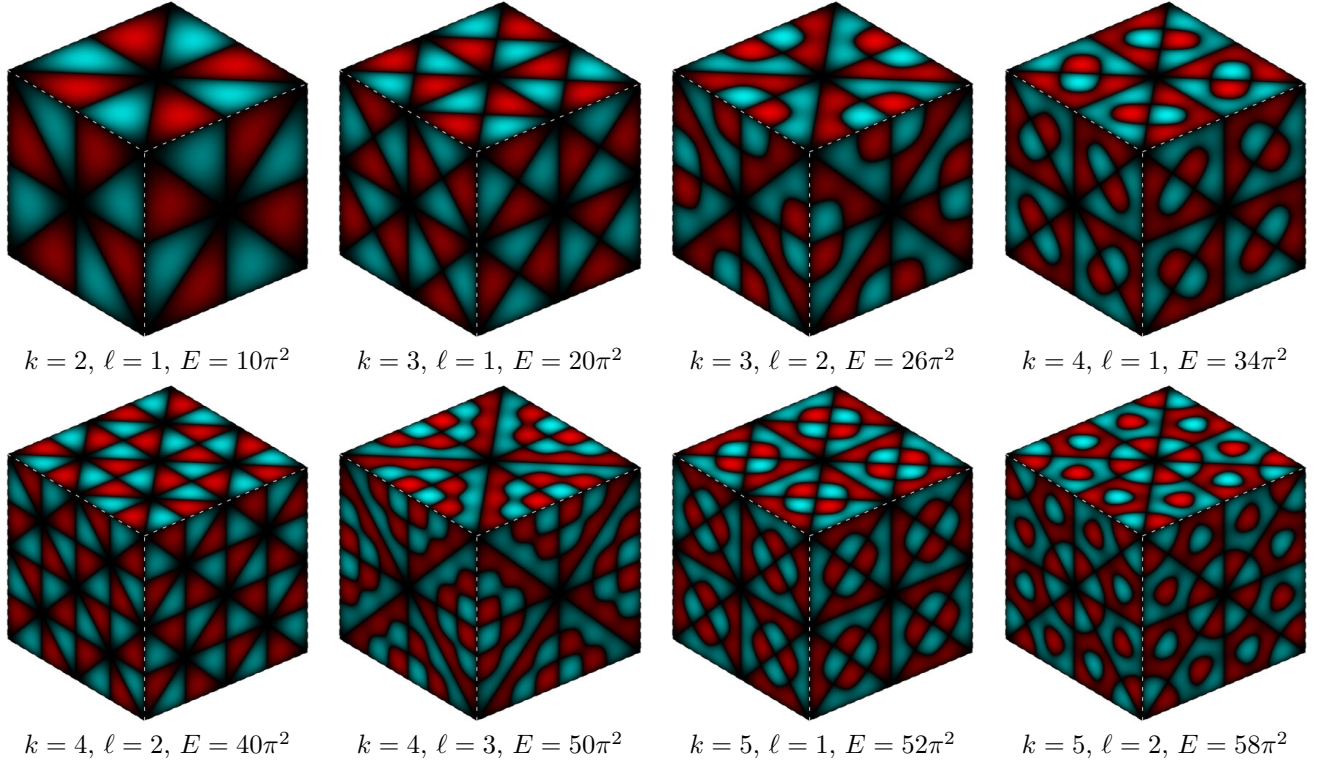


FIG. 13. The first eight modes for the irreducible representation A_{1u} .

of negative Dirac δ -potentials on the cube edges, which would cause jumps of the normal derivatives of the wavefunction when going from one cube face to another, and complicate the boundary conditions slightly. However, the mathematical structure of the problem would essentially remain the same, in particular the hierarchy of the solutions and their degeneracies stemming from the irreducible representations of the octahedral group. Moreover, the modes corresponding to the irreducible representations A_{1u} and A_{2g} would be the same as described in this paper because they are zero on the cube edges, so they would not be altered by the additional delta potential on the edges. Analysis of the remaining modes will be subject of future research.

Appendix A: Numerical calculation of coefficients in Eqs. (7), (8), (9) and (11)

In this Appendix, we give a more detailed explanation of the numerical procedure we employed to find the energies and modes for the degenerate cases.

For concreteness, let us consider the two-dimensional representation E_g . We have obtained a series for the basis functions φ and ψ ; φ is given by Eq. (7), and ψ is related to it as $\psi(x, y) = \varphi(x, y)$. The series contains unknown coefficients c_k and the unknown energy E . To find them, we employ the boundary condition $\left. \frac{\partial}{\partial y}(\psi - 2\varphi) \right|_{y=1/2} = 0$. Plugging in the series representations, we rewrite this

condition as $\sum_{k=0}^{\infty} c_k g_k(x; E) = 0$ for all $x \in [0, 1]$, where

$$g_k(x; E) = -(-1)^k (2k+1)\pi \cos \left[\sqrt{2E - (2k+1)^2 \pi^2} x \right] + 2\sqrt{2E - (2k+1)^2 \pi^2} \sin \frac{\sqrt{2E - (2k+1)^2 \pi^2}}{2} \times \cos [(2k+1)\pi x]. \quad (\text{A.1})$$

This is effectively a homogeneous linear system for c_k . For almost all values of E , the g_k will be linearly independent and there will only be a zero trivial solution. Hence, we must search for E for which the g_k are dependent.

Such a search is most easily performed if the functions $g_k(x)$ are expanded in a suitable basis. In that case, g_k can be replaced by a vector of its coefficients, and the problem is reduced to establishing linear dependence of vectors with numerical entries. To find a good basis, we notice that $\left. \frac{\partial \psi}{\partial y} \right|_{y=1/2}$ is a series in $\cos[(2k+1)\pi x]$, and that $2 \left. \frac{\partial \varphi}{\partial y} \right|_{y=1/2}$ must be equal to it, so $\left. \frac{\partial \varphi}{\partial y} \right|_{y=1/2}$ must also be expandable into a series of this form. Hence $\sum c_k g_k$ can be expanded like this too. Furthermore, the functions $2 \cos[(2k+1)\pi x]$ are orthonormal on the interval $[0, 1/2]$ with respect to the inner product $\int_0^{1/2} f^* g dx$, so they form the basis we are looking for. All of this makes it reasonable to expect that g_k can be written as

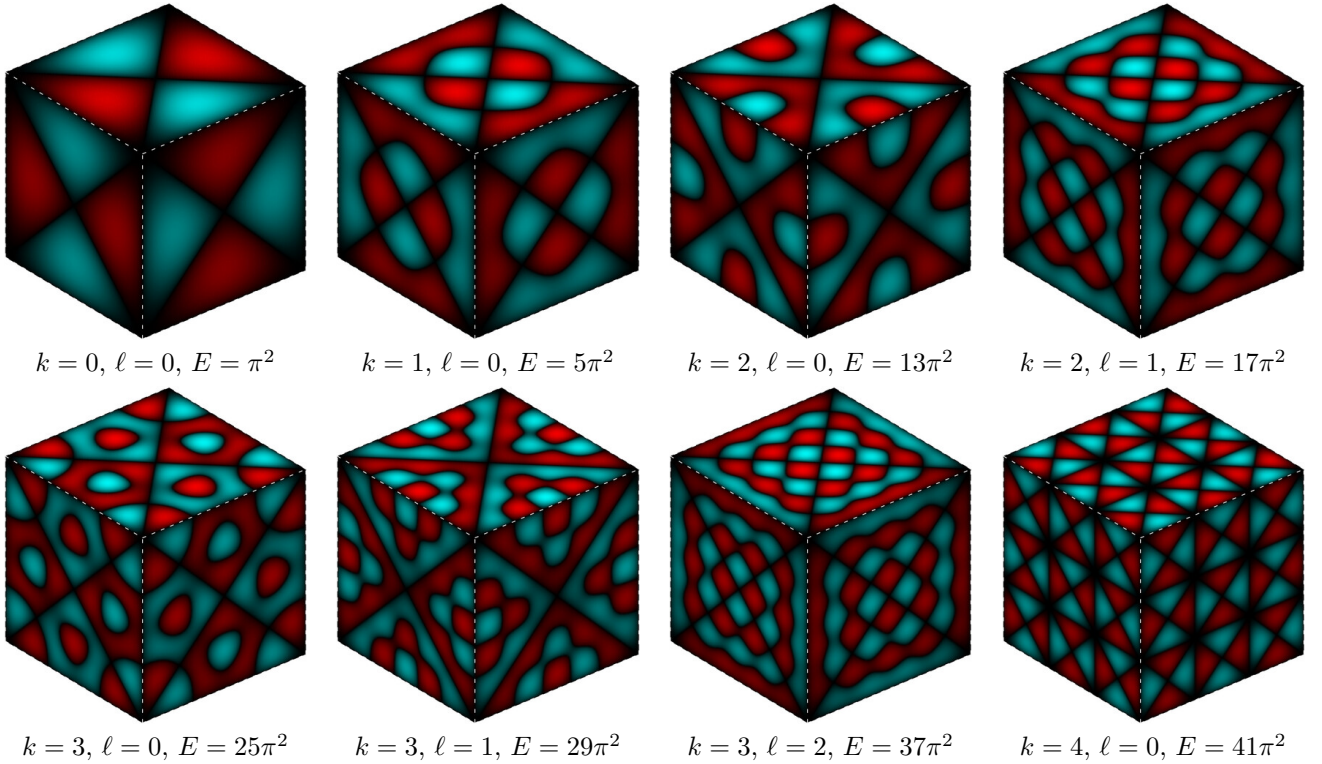


FIG. 14. The first eight modes for the irreducible representation A_{2g} .

$\sum_{n=0}^{\infty} G_{kn} \cos[(2n+1)\pi x]$, where

$$G_{kn} = 4 \int_0^{\frac{1}{2}} g_k(x; E) \cos[(2n+1)\pi x] dx. \quad (\text{A.2})$$

This means that each g_k can be represented by an (infinite) vector of its coefficients G_{kn} . The energies are now determined as the values of E that make the (infinite) set of vectors G_{kn} linearly dependent.

In practice, it turns out that we can truncate this infinite system and still get good results. This is because in most of the g_k , the $\cos \sqrt{(\dots)}x$ will in fact turn into a cosh as discussed in Sec. V, producing evanescent terms. In other words, the “superoscillatory” behavior of the term in the y direction will be compensated by its exponential behavior in the x direction. However, with an increasing “evanescent wavenumber” the derivative picks up a factor corresponding to the wavenumber, so the evanescent terms have to decrease quickly, and usually truncating the series after just three evanescent terms gives excellent results.

We further proceed in this fashion: we break the positive half-line $[0, \infty)$ of energies E into smaller intervals, so that on each of them, the number of terms with ordinary (not hyperbolic) cosines in the expansions of φ and ψ is constant, i. e. $(0, \pi^2/2)$, $(\pi^2/2, 9\pi^2/2)$, $(9\pi^2/2, 25\pi^2/2)$ etc. Each of these intervals is then processed separately: we truncate the expansion of g_k so that it contains all the ordinary cosines, and the given constant number (in our

case, three) of the hyperbolic cosines (evanescent terms). Then we calculate the same number of coefficients G_{kn} for each g_k . This yields a square matrix G_{kn} whose coefficients depend only on the energy.

Now we must find the values of E in the given interval for which the truncated matrix G_{kn} is close to having less than full rank. To this end, we employ the singular value decomposition: we numerically find the least singular value of G_{kn} for many energies in the interval and look for local minima. The neighborhoods of such minima are then searched again in a more fine manner, and this refinement is repeated several times. The resulting positions of the local minima are the required energies, and the corresponding singular vectors give the coefficients c_k that can be used to construct the mode. This is repeated for as many intervals as we please.

The modes and energies of all other representations can be found in the same manner. In each of the other cases, the expansions are slightly different, but the process itself remains the same. The biggest difference occurs for the triple-degenerate modes where there are two sets of coefficients (c_k that characterize the function f , and d_k that do the same for the function g) and two conditions instead of one. However, we can still expand both functions to the same number of terms N , which gives $2N$ unknown coefficients, and similarly, both conditions can be Fourier-expanded to N terms, which gives $2N$ equations. The solution mechanism remains the same, apart from the fact that the matrices have bigger dimensions.

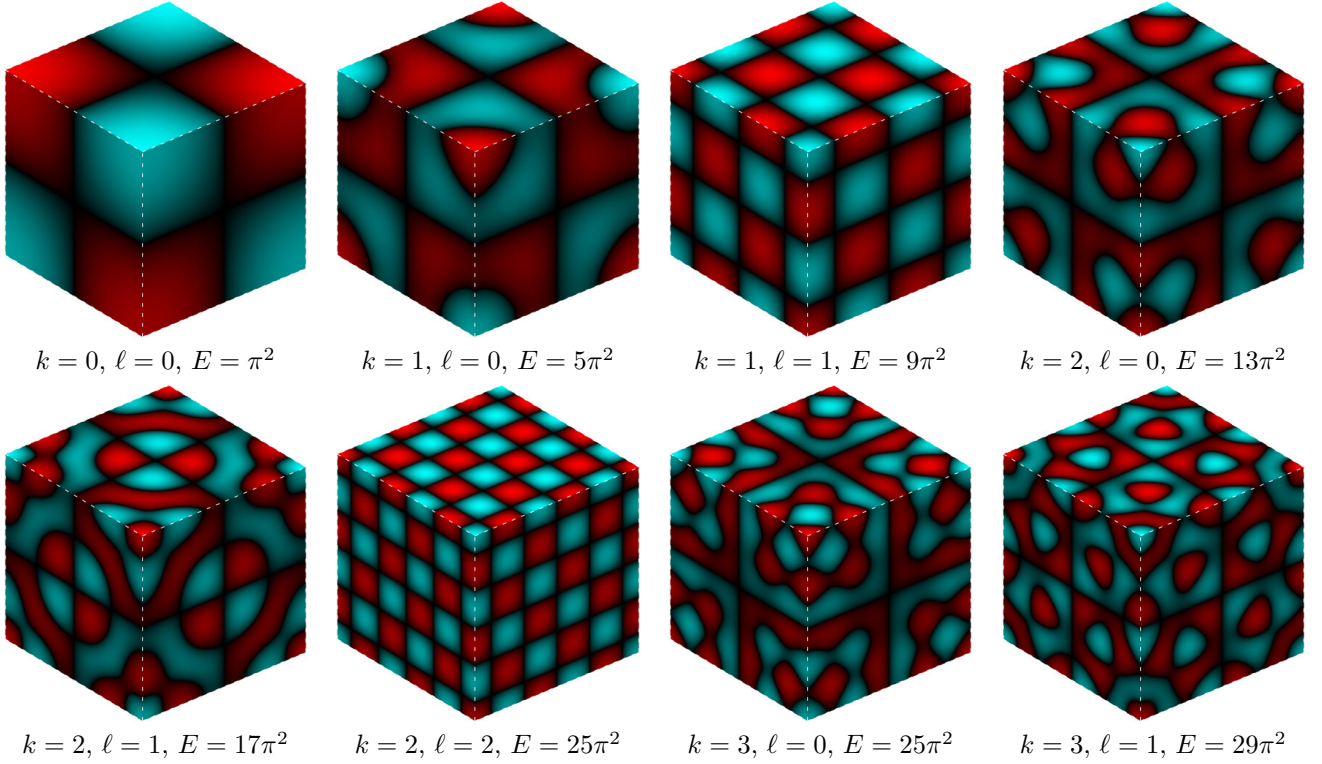


FIG. 15. The first eight modes for the irreducible representation A_{2u} .

-
- [1] M. Kac, Can One Hear the Shape of a Drum?, *Am. Math. Monthly* **73**, Part 2, 1–23 (1966).
- [2] E. Gutkin, Billiard dynamics: An updated survey with the emphasis on open problems, *Chaos* **22**, 026116 (2012).
- [3] O. Bohigas, M. J. Giannoni, and C. Schmit, Characterization of Chaotic Quantum Spectra and Universality of Level Fluctuation Laws, *Phys. Rev. Letters* **52**, no. 1 (1984).
- [4] R. C. T. da Costa, Quantum mechanics of a constrained particle, *Phys. Rev. A* **23**, 1982–1987 (1981).
- [5] J. Bě́lín, S. Horsley, and T. Tyc, Quantum mechanics and Talbot revivals on a tetrahedron, *Phys. Rev. A* **100**, 033806 (2019).
- [6] J. Bě́lín, T. Tyc, and S. Horsley, Optical simulation of quantum mechanics on the Möbius strip, Klein’s bottle and other manifolds, and Talbot effect, *New J. Phys.* **23**, 033003 (2021).
- [7] D. G. Garcia, G. J. Chaplain, J. Bě́lín, T. Tyc, C. Englert, J. Courtial, Optical triangulations of curved spaces, *Optica* **7**, 142 (2020).
- [8] M. Šarbort and T. Tyc, Spherical media and geodesic lenses in geometrical optics, *J. Opt.* **14**, 075705 (2012).
- [9] L. Xu, X. Wang, T. Tyc, C. Sheng, S. Zhu, H. Liu, and H. Chen, Light rays and waves on geodesic lenses, *Photonics Research* **7**, 1266 (2019).
- [10] Y. Shen, X. Wang, Z. Xie, C. Min, X. Fu, Q. Liu, M. Gong, and X. Yuan, Optical vortices 30 years on: OAM manipulation from topological charge to multiple singularities, *Light: Science & Applications* **8**, 90 (2019).
- [11] J. H. Hannay and A. Lockwood, The quantum Talbot effect on a sphere, *J. Phys. A: Math. Theor.* **41**, 395205 (2008).

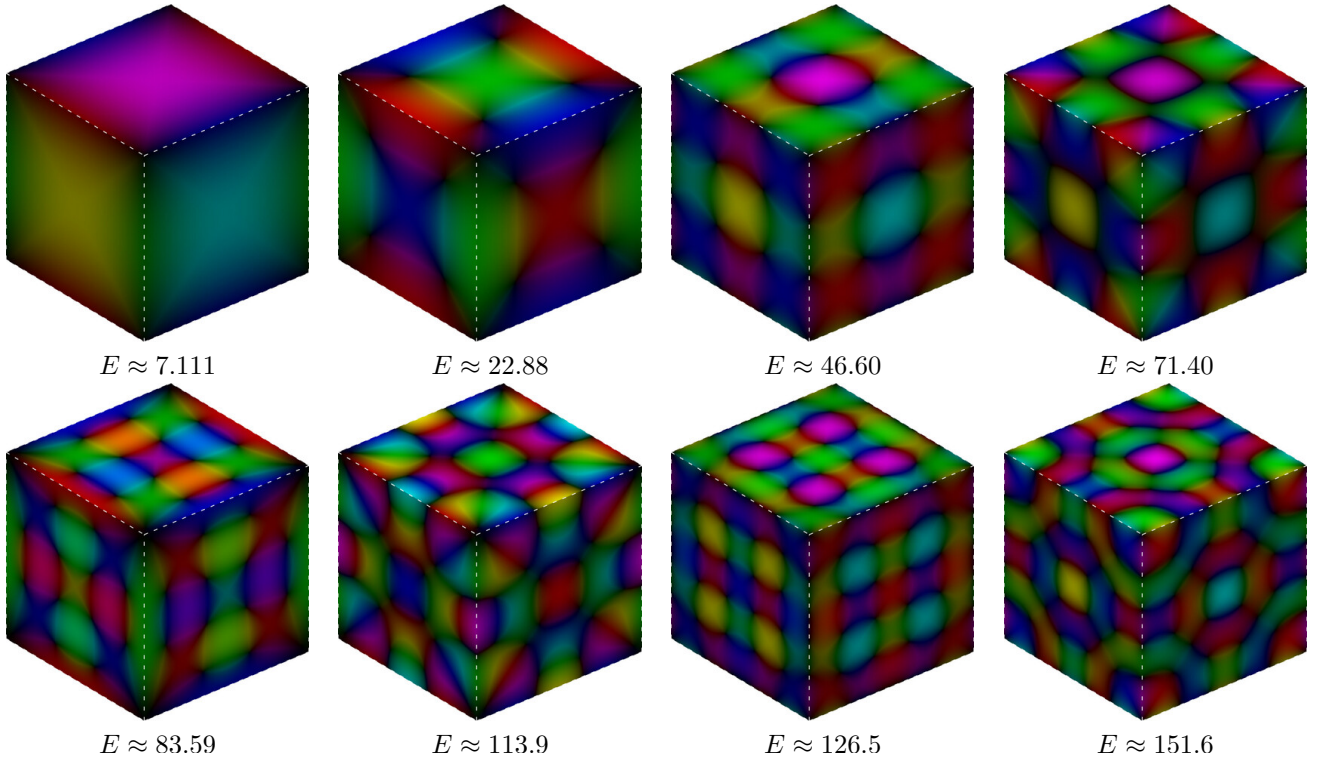


FIG. 16. The first eight modes for the irreducible representation E_g . A vortex is formed at each cube vertex.

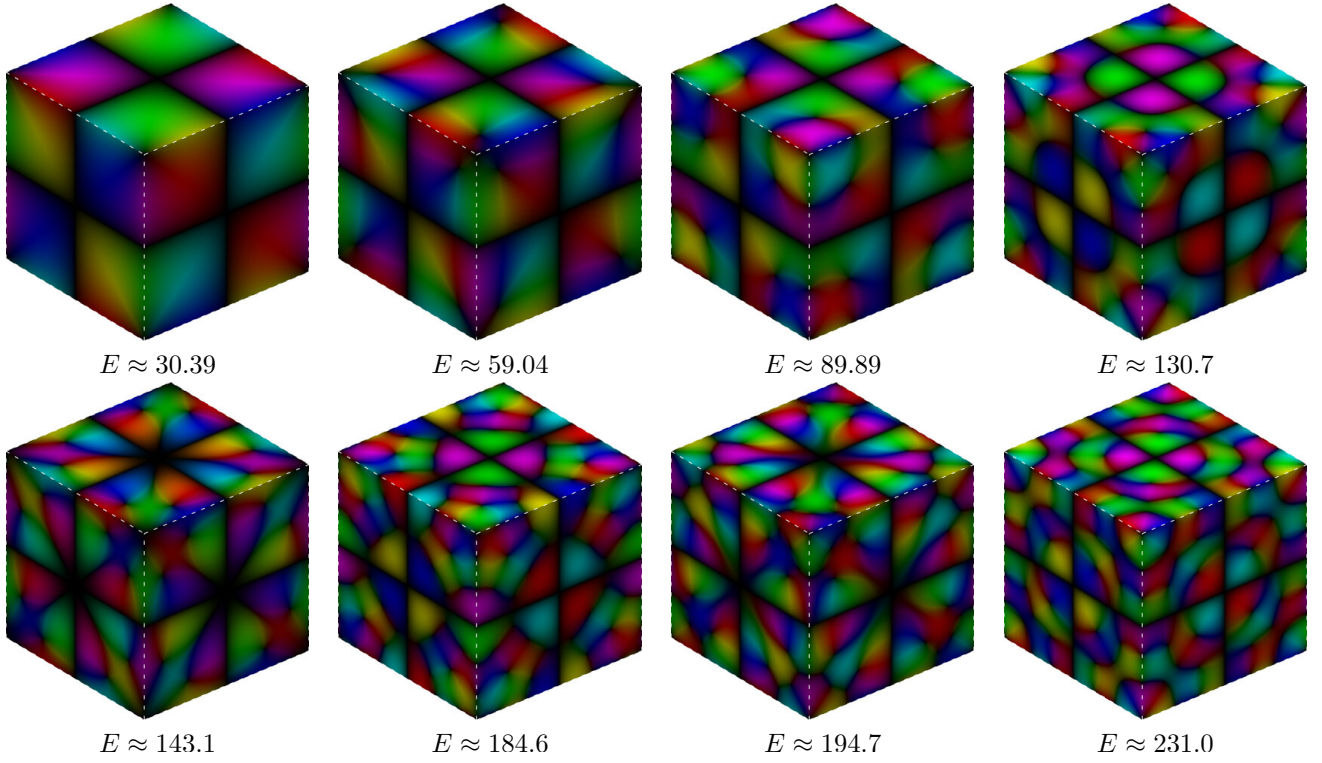


FIG. 17. The first eight modes for the irreducible representation E_u . A vortex is formed at each cube vertex.

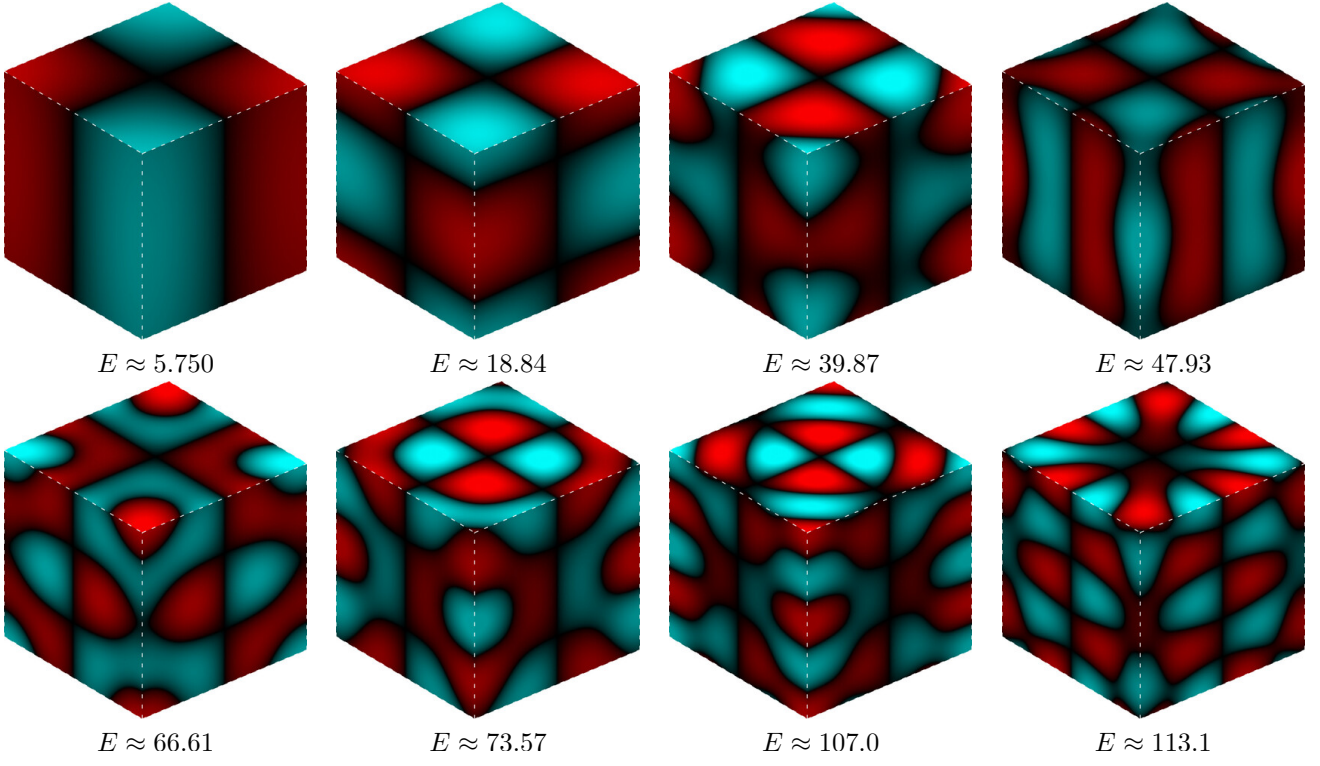


FIG. 18. The first eight modes for the irreducible representation T_{1g} .

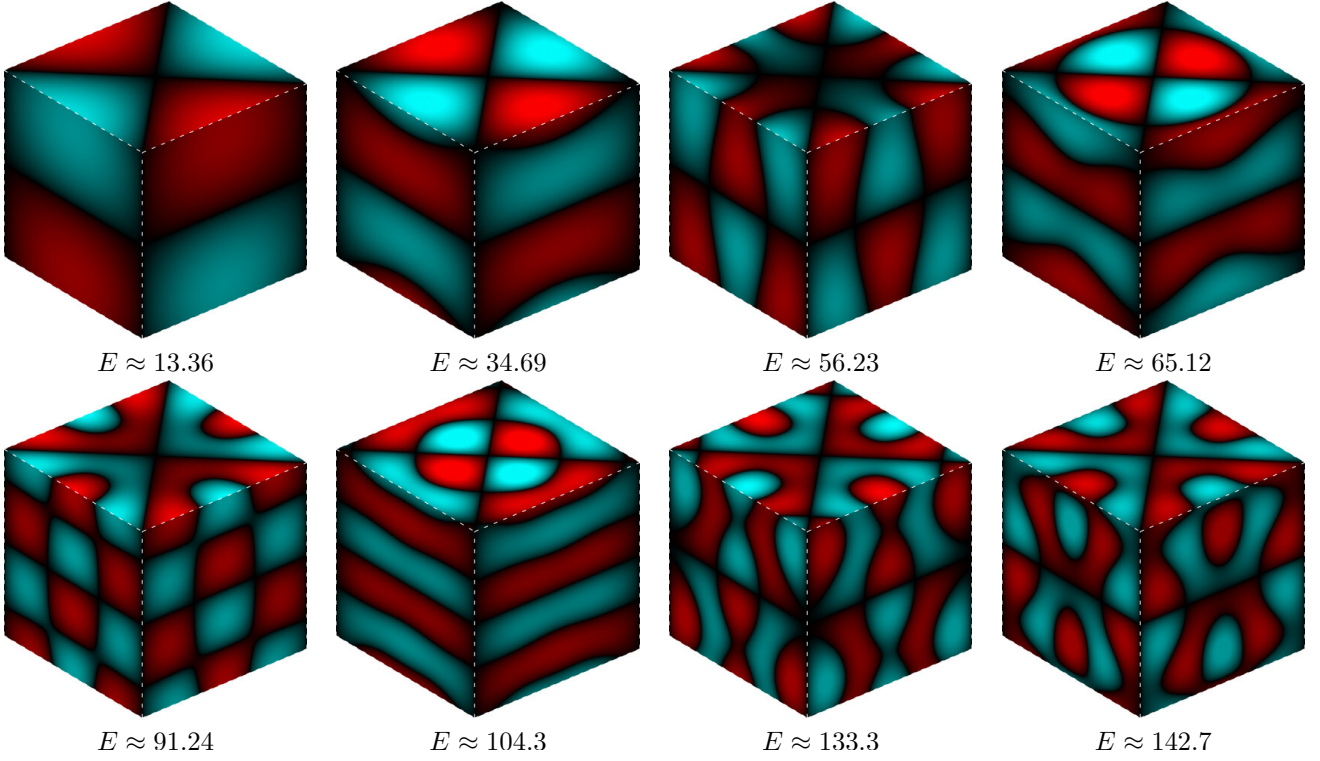


FIG. 19. The first eight modes for the irreducible representation T_{1u} .

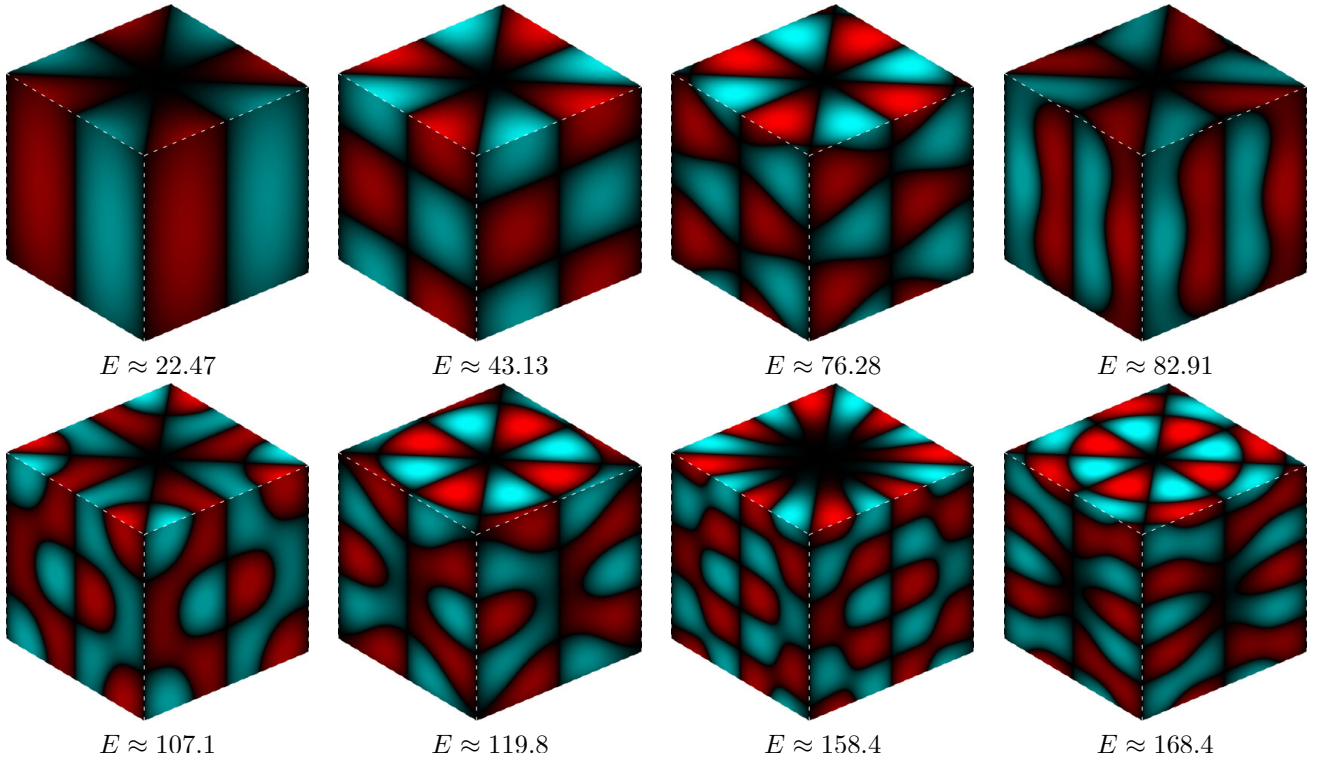


FIG. 20. The first eight modes for the irreducible representation T_{2g} .

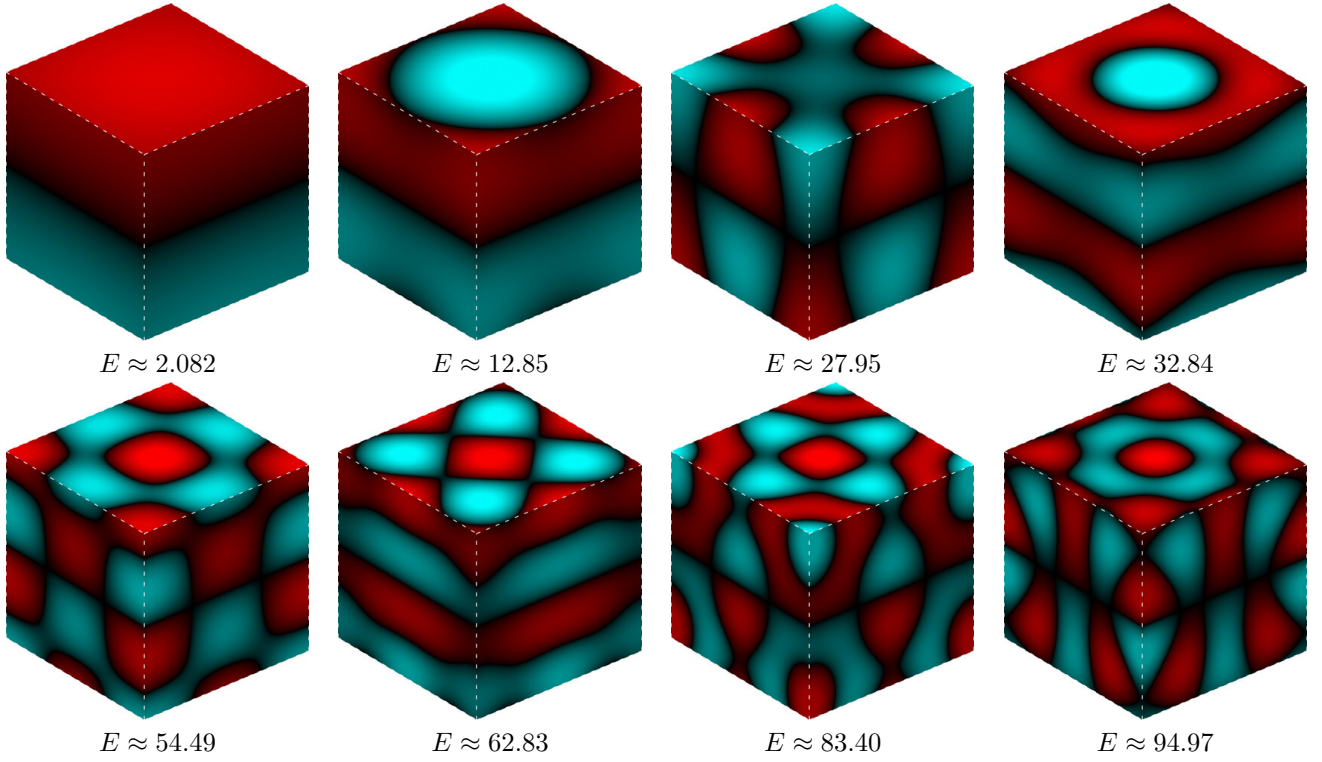


FIG. 21. The first eight modes for the irreducible representation T_{2u} . The wavefunction on the bottom polar face (unseen) is the negative of the one on the upper polar face.